Research Article

On-site reduction of nitrogen oxides at an emission hotspot using actively vented photocatalytic reactors in a highway tunnel

Clemens Ehm[1] · Max O. Frohmüller[1] · Thomas Flassak[2] · Dietmar Stephan[1]

Received: 17 October 2021 / Accepted: 4 April 2022
Published online: 25 April 2022

Abstract

This study presents our solution of an active nitric oxides (NO_x) control method for large traffic tunnels. A titanium dioxide (TiO_2) coated carrier material is assessed using lab-based photocatalysis experiments, leading to a coating with high photocatalytic activity (deposition speed of 1.4 cm/s for nitrogen monoxide, NO). The coating is tested on several carrier materials to maximize the interaction between the reactive surface and the pollution molecules in the air. Several reactor prototype geometries and carrier materials are simulated and tested on a pilot plant scale. A coated PU-foam with 3 cm thickness and porosity of five pores per inch proved to be the most effective carrier material, while a reactor design with vertically flowed stacks of the foam carrier is capable of optimally exploiting the potential of the photocatalytic coating for high volume flows. With data from on-site measurements of the atmospheric conditions and pollution in the highway tunnel 'Rudower Höhe' in Berlin, Germany, we could build a simulated tunnel setup of our reactors within the tunnel. An estimate based on these simulations assumes a reduction potential of 25% of the NO_x mass generated in the tunnel. In conclusion, actively vented TiO_2 surfaces are controversial yet could achieve high removal rates while simple to clean or exchange.

Article Highlights

- This study shows the persisting situation of very highly polluted air with on-site measurements in a road tunnel near Berlin (Germany).
- We investigate the solution approach to clean the tunnel air by oxidizing and fixating pollutants with photocatalysts before the air is released off the tunnel.
- We can show that about 25% of nitric oxides produced due to the traffic in the tunnel can be removed with a combination of active ventilation and photocatalytic depletion.

Keywords NO_x hotspot · Photocatalysis · Highway tunnel · Catalytic oxidation · On-site reduction · TiO_2 · Active ventilation

Supplementary Information The online version contains supplementary material available at https://doi.org/10.1007/s42452-022-05035-7.

✉ Dietmar Stephan, stephan@tu-berlin.de; Clemens Ehm, clemens.ehm@tu-berlin.de; Thomas Flassak, thomas.flassak@lohmeyer.de | [1]Department of Building Materials and Construction Chemistry, Technische Universität Berlin, Berlin, Germany. [2]Lohmeyer GmbH, Karlsruhe, Germany.

1 Introduction

Nitrogen oxides remain a sociopolitical issue in Germany and Europe as their ambient concentrations continue to exceed the limit values for years [1–5]. Especially nitrogen dioxide (NO_2) is hazardous for human health. The effects of chronic burdens may reach from the state deterioration of asthma patients to lung dysfunction and cardiovascular effects, whereas the latter two were observed with insufficient significance [6, 7]. Additionally, nitrogen oxides can lead to the formation of tropospheric ozone [8, 9], which is highly toxic towards humans and the environment [10, 11]. NO_x leaves the atmosphere via wet deposition, forming HNO_3 and thus contributing to soil acidification [12].

The sharp decrease of NO_x-related air pollution levels in the wake of COVID19-pandemic and its following traffic decline [13–16] has clearly illustrated that limit value exceeding NO_x are caused by human activities and can be held in check. Different long-term solutions, such as electric drive systems or technology advancements in fuel combustion engines, promise to greatly alter on-road fleet emission characteristics towards nitrogen- and carbon-poor profiles [17–19]. However, these projections observe time frames up to 30 years from now, making efficient short-term solutions seem desirable. Furthermore, immediate action seems necessary, given that at least 40 mil. people were exposed to NO_x concentrations above the annual limit between 2003 and 2012 in the EU alone (EU estimate: 8%—27% of inhabitants) [12].

Many studies have proven the ability of TiO_2 to catalyze NO_x under the presence of UV-light since it was first described [20]. Serpone has reviewed those developments in extensive detail and summarized over 30 years of research on this topic in his work, which should be consulted for further reading [21]. Among other things, the author concluded that a key problem of present-day applications is the lack of transferability from laboratory experiments to field implementation, especially regarding surface passivation/blockage, reformation of NO_x on the catalytic surface, incident flow, irradiation spectra, resident times, and the carrier's ratio of active surface and volume. The latest research focusing on TiO_2 application as an additive for concrete or as a coating on carrier materials in various forms, such as TiO_2 nanotubes, shows potential to enhance durability and future projects will need to address these difficulties [22–25].

Upon activation by UV-light, an electron of TiO_2 is transferred to the conduction band, leaving a p-hole in the valence band (Eq. 1). This triggers a series of reactions involving NO_x, O_2 and H_2O, which can be simplified as shown in Eqs. 2 and 3 [26]. Ultimately, the reaction forms adsorbed nitric acid or nitrate anions, which will adhere to the surface until washed off by water [26, 27].

$$TiO_2 \xrightarrow{+h\nu} h^+_{vb} + e^-_{cb} \tag{1}$$

$$2NO + O_2 \xrightarrow{+h\nu,TiO_2} 2NO_2 \tag{2}$$

$$2NO_2 + H_2O + 0.5O_2 \xrightarrow{+h\nu,TiO_2} 2HNO_3 \tag{3}$$

These processes make TiO_2 a viable catalyst for outdoor application, where UV-irradiation is readily provided by the sun and large surfaces are available, especially in urban areas. Yet, field applications suffer insufficient durability and effectiveness, as said before. These problems can perhaps be addressed within a more technical field implementation, particularly at emission hotspots, since surface passivation by heavy pollution can completely shut off NO_x reduction, which was demonstrated at 'Leopold II' tunnel in Brussels [28]. Such an implementation could actively aspirate air, guiding it over an artificially UV-irradiated material with a high surface-volume-ratio. In this way, undefined incident flows, irradiation spectra, resident times, and carrier surface-volume rations would be avoided [21], which could also lower diffusive and convective transport resistances towards the TiO_2-faces. Furthermore, those materials could be washed or exchanged periodically to counteract surface passivation and blockage. On the other hand, active ventilation and irradiation consumes energy in operation, which perhaps results in more secondarily emitted NO_x than purified in the process. Consequently, the scope of this work was to assess the best approach for a high NO_x reduction potential, considering both actively and passively vented TiO_2-coated surfaces for a specific hotspot.

As an example of an anthropogenic NO_x hotspot, the 'Rudower Höhe' highway tunnel in Berlin has been chosen as the test side in this study. Week-average NO_x burdens were determined in the field and used as a basis for simulations, aiming to find a best practice approach for on-site reduction applications. Additionally, the construction of a TiO_2-coated foam reactor supplied necessary data to estimate an upper reduction limit by actively vented high-surface materials.

Road-traffic tunnels are artificial spaces connected to the open atmosphere but underlie significantly altered conditions. In the absence of UV radiation, photolytic reactions are halted, and polluted air cannot be exchanged with fresh air over the length of the tunnel. Thus, oxidants such as ozone exist in limited amounts and are consumed during the traverse. Other pollutants (CO, CO_2, NO_x, particulate matter, and VOC) are constantly emitted by the passing vehicle fleet and

accumulate in the tunnel air. High pollution loads by tire and brake abrasion generate a layer of dust on all surfaces, which is generally challenging for all technical equipment but especially for analytical instruments as used in this project [21, 28–30].

The tunnel air stream determines pollutant accumulation, which depends on the tunnel model, traffic volume, and vehicle speed. It also poses a considerable safety risk. A review of the Australian NHMRC recommended additional ventilation for all tunnels longer than 300 m to meet these risks [30]. Tunnels over 600 m would need transverse/semi-transverse systems, which transport fresh air into the tunnel. Similar regulations are formalized in the German RABT guidelines, which allow active ventilation for highly frequented tunnels up to 600 m, or up to 1,200 m length after a risk assessment [31]. Facilities with a greater extent would require ingoing vent lines to provide fresh air. Therefore, the strongest pollutant accumulation (in Germany) could probably be found in tunnels the length of 1 km without such features.

Fleet emissions include numerous pollutants, such as CO, CO_2, NO_x, particulate matter, and VOC (like aldehydes, polycyclic hydrocarbons, and BTEX) [32]. Nitrogen oxides are mainly emitted as nitrogen monoxide, which can be converted to nitrogen dioxide under consumption of an oxidant (Eq. 4), whereas VOC can form peroxide radicals with OH radicals (Eqs. 7 and 9) and act as oxidant as well (Eqs. 8 and 10). Since neither an exchange with fresh air is possible nor an ozone formation reaction (Eqs. 5 and 6) can take place without UV-light, ozone, OH radicals, and peroxide radicals are rapidly depleted inside the tunnel. Therefore, CO, CO_2, NO and VOC concentrations rise over the tunnel length, while NO_2 levels increase slowly. This causes the NO_2/NO ratio decreases until NO concentrations of more than 2 ppm are reached, above which the NO_2 formation from nitrogen monoxide and oxygen (Eq. 11) becomes relevant [8, 11, 29].

$$NO + O_3 \rightarrow NO_2 + O_2 \quad (4)$$

$$NO_2 + h\vartheta \rightarrow NO + O \quad (5)$$

$$O + O_2 + M \rightarrow O_3 + M \quad (6)$$

$$RH + OH + O_2 \rightarrow RO_2 + H_2O \quad (7)$$

$$RO_2 + NO \rightarrow RO + NO_2 \quad (8)$$

$$RO + O_2 \rightarrow R'CHO + HO_2 \quad (9)$$

$$HO_2 + NO \rightarrow OH + NO_2 \quad (10)$$

$$2NO + O_2 \rightarrow 2NO_2 \quad (11)$$

In total and relative to the open atmosphere, high NO and VOC concentrations and a low NO_2/NO ratio can be expected at the tube exit, which, combined with sufficient UV-irradiation intensity, lead to tropospheric ozone formation [8, 30]. These attributes show why tunnels are most suitable for active air cleaning methods, as traffic emissions are virtually integrated over the tunnel length and set free at a single point.

The publication consists of parts that build onto each other. On-site measurements reflect the condition in the tunnel and serve as a basis for simulation calculations. Laboratory measurements at standard conditions were used to develop a photocatalytically active coating which was then used on different base materials in the reactors. CFD calculations were performed in parallel with pilot plant tests to find an optimal internal structure of the reactors. Finally, CFD simulations optimized the reactor placement in the tunnel tube to realize maximum pollutant removal.

2 Materials and methods

2.1 Study area 'Rudower Höhe'

All experiments regarding zero measurements of a highway tunnel emission profile were conducted between 2014 and 2015 at the 'Rudower Höhe' highway tunnel, which belongs to Bundesautobahn A113 and lies in the south-west of Berlin. The tunnel consists of 2 separated tubes with unidirectional traffic, which are approx. 1 km long, 15 m wide (see Fig. S1, Online Resource 1) and highly frequented with 20,000 to 50,000 vehicles per day, respectively [32]. Both tubes are ventilated with jet fans [31].

Three individual measurement containers were set up in the westerns tube, placed at the entrance, the exit and halfway through the tube. Each one of them contained one API Teledyne Modell T200 (NO, NO_2 and NO_x monitoring) and one API Teledyne Modell T360 (CO_2 monitoring). The tube exit container also included an integrated weather station by Lufft, which determined temperature, humidity, wind speed and direction, and pressure. All instruments were mounted to the outer wall and sampled at 2.5 m height.

The NO_x and CO_2 measurement took place at minute intervals over multiple weeks at the end of 2015. Due to reoccurring instrument failures caused by heavy contamination with tire abrasion or similar traffic-originated residues, continuous NO_x and CO_2 data could only be obtained in the 51. calendar week. Measurement data from other weeks as well as all PM measurements did not match standards of quality and are not presented in this

work. Therefore, measured NO_x and CO_2 burdens have been interpreted as a possible rather than a typical emission profile of the tunnel. Temperature, humidity, and wind speed/direction measurements were carried out between November 2014 and February 2015.

Following the presented theory on NO_x inside highway tunnels, it was assumed that pollution levels inside the tunnel are to correlate with the volume of traffic. As significant differences between workday and weekend traffic volumes have been expected, the minute-wise data were separately averaged for workdays and weekends.

2.2 Theoretical NO_x reduction potential

The application in this study works with the concept of a substrate for mechanical support combined with a coating containing the photocatalyst. Mechanical support was provided by a 5 ppi (*pores per inch*) polyurethane (PU) foam made by Eurofoam (Bulpren C 28,800 EC). Two approaches for coatings were examined, a cementitious and a dispersion one. While similarly high photocatalytic activity was found possible in both systems in this project, the dispersion coating had advantages regarding availability and processability. Therefore, only experiments with dispersion coatings are presented in the following.

To estimate the catalytic capability of TiO_2 coated permeable materials, a small polymethyl methacrylate (PMMA) reactor was built (see Fig. S2, Online Resource 1). The reactor holds a 5 ppi (*pores per inch*) specimen with a size of 0.1 m × 0.1 m × 0.03 m. The airflow was forced to penetrate the foam by the geometrics of the PMMA-reactor. On the inlet and outlet side, the foam was irradiated with 10 ± 1 W/m^2 365 ± 5 nm ultraviolet (UVA) light. The irradiation was produced by an array of ultraviolet light-emitting diodes (UVED) of the type Nichia NSSU100C and determined inside the reactor at the level of the surface of the foam. Additionally, sensors for temperature, humidity, pressure, and UV-intensity were integrated on the inner side of the reactor cover to surveil the reaction parameters.

To estimate the long-term performance of the photocatalytic coating, a long-term measurement was conducted over 32 days using a photocatalytically coated foam. Ambient air of the departments workshop was aspirated through the PMMA reactor with 17 l/min, while in- and outgoing air were continuously sampled with Horiba APNA 360 NO_x monitors. All data have been averaged over 30 min intervals to ease analysis.

A follow-up analysis of the amount of nitrate, which forms during catalysis (Eqs. 1–3), has been used to verify the measurement. The foam was washed two times with 100 ml deionized water. Both solutions were combined and twice quantified with a Metrohm 761 Compact Ion Chromatography device.

2.3 Influence of reaction surface geometry

To further assess the possible purification capability of photo-catalytical active surfaces at the study site 'Rudower Höhe', CFD simulations were carried out for two TiO_2-coated material geometries. The two prototypes are orientated on a different approach in the field, respectively. While prototype A constitutes the application of photo-catalytically active, perfusable nets near the tunnel walls, prototype B follows a fundamentally different design idea. It represents the installation of reactor cassettes at the side of the road. Those cassettes would need to actively aspirate air from the tunnel over as much foam surface as possible. Aside from these preliminary considerations, both prototypes were simulated as reactor cassettes, as the most practical application (actively or passively vented) could only be discussed based on their efficiency, pressure drop, and tunnel airflow profile. Furthermore, these prototypes were built in real scale. The experimentally determined nitric oxide depletion efficiency was compared to the simulation results.

All simulations are created with Phoenics software [33] and aim to estimate various coefficients. First off, the non-diffusion-limited degradation rate (NDR) is analytically calculated under the assumption of neglectable transfer resistances on the fluid's side. It is furthermore hypothesized, that the degradation inside the prototype would be proportional to the concentration. The following dependency (Eqs. 12–14) between inlet and outlet concentration is derived from fundamental photocatalytic reaction kinetics [34]. S_{TK} is the active surface in m^2, V_{TK} is the prototype volume in m^3, V is volume flow in m^3/s and v_d is the deposition velocity, which is assumed to be 1.4 cm/s for all simulations based on photocatalytic tests with the coating material according to ISO 22197–2. As a base for the chemical kinetics, the chemistry of a plug flow reactor is assumed to dominate the reactor prototypes. With rising volume flow, the error is estimated to be increasingly negligible.

$$\frac{c_{out}}{c_{in}} = e^{-k_{TK} \cdot t_{reaction}} \tag{12}$$

$$\text{with}: \quad k_{TK} = v_d \cdot \frac{S_{TK}}{V_{TK}} \tag{13}$$

$$\text{and}: \quad t_{reaction} = \frac{V_{TK}}{\dot{V}_{TK}} \tag{14}$$

The NDR coefficient, hence the concentration difference between inlet and outlet referred to the inlet concentration, was calculated with Eq. 16.

$$NDR = \frac{\left(c_{in} - c_{out}\right)}{c_{in}} = 1 - \frac{c_{out}}{c_{in}} \quad (15)$$

$$NDR = 1 - e^{-v_d \cdot \frac{S_{TK}}{\dot{V}_{TK}}} \quad (16)$$

The arising 'pollution removal mass flow', expressed as the reduction rate times the volume flow times the inlet concentration ($NDR \cdot \dot{V}_{TK} \cdot c_{in}$), was used to assess the prototypes' degrees of efficiency. The value was divided by the maximal possible removal mass flow, expressed as photocatalytic surface times the deposition velocity times the inlet concentration, to receive a dimensionless coefficient η (Eq. 17).

$$\eta = \frac{NDR \cdot \dot{V}_{TK} \cdot c_{in}}{S_{TK} \cdot v_d \cdot c_{in}} \quad (17)$$

The *realistic degradation rate* (RDR), which was the proportion of NDR reached and the pressure drop, had been numerically estimated by the simulations. All presented coefficients were crucial to assessing the possible application concepts arising from the prototypes. To achieve a high cleaning performance, RDR should be near 100%, while NDR and the degree of efficiency would need to be considered together. As the degree of efficiency is expressed in reference to the inlet concentration, it may become maximal when the volume flow is high, and the concentration drop over the reactor is low since, in this way, the concentration difference between the active surfaces and the free fluid stays steep over the whole reactor. Yet, high throughput rates would cause the c_{in}–c_{out} term, and thus the NDR, to become minimal.

The pressure drop can express how much the purification efforts would slow the tunnel or the reactor air stream, which is a safety issue and affects the degree of efficiency, as already laid out. Furthermore, a prototype with a minimal pressure drop can perhaps remove large NO_x masses without active ventilation. This could lower cost and lighten the ecologic footprint of the application itself.

The simulation of prototype A (Figure S3, Online Resource 1) had been done at an early stage of this work and was initially computed with a volume flow of only 30 m^3h^{-1} in contrast to prototype B (Figure S4, Online Resource 1), which assumed 400 m^3h^{-1}. Thus, the results of this simulation may not be directly compared, although the NDR and RDR coefficients are closer related to the surface-to-volume-ration, which is, within limits, independent from the inner surface. The reactor layout had a surface-volume-ratio of 44 m^2m^{-3} and was designed with 5 perfusable mesh grid tubes the length of 1.5 m and 0.15 m in diameter.

Prototype B sought to achieve a high surface-volume-ratio, as this prototype was thought to represent the installation of actively vented reactors in the tunnel. Nevertheless, to keep the pressure drop low, TiO_2-coated foam pads with a thickness of 30 mm and a pore density of 5 ppi were used, as tested in the laboratory PMMA reactor. This resulted in a surface-volume-ratio of 78 m^2m^{-3}. The pads were installed perpendicular to the flow direction so that polluted air was forced to penetrate the foam body.

2.4 Internal air flow and concentration profiles

In the last step, airflow and concentration profiles were simulated for the tunnel 'Rudower Höhe' under non-stationary conditions. The simulation space is shown in Figure S5 of Online Resource 1. It was intended to visualize the air movements and flow parameters, to estimate and compare the serviceability of passively and actively vented photocatalytic surfaces since passive ventilation would need to rely on a turbulent flow, which constantly and, more important, quickly exchanges purified air from the reaction surfaces with polluted air from the road. It furthermore remained in question if such an exchange can be induced with active ventilation.

The first simulation included 24 different vehicles on three lanes with 4 heavy-duty vehicles (HDV) and 20 light-duty vehicles (LDV). HDVs on the right-hand lane were included with an assumed traveling speed of 80 km/h, LDV travel speed was 85 km/h on the middle lane and 90 km/h on the left-hand lane (everything in travel direction). The calculation aimed to estimate air flow and concentration profiles in the tunnel in the observed time window. The piston effect, as well as vortex formation and exhaust emissions, were observed separately for every vehicle, but their aerodynamic features were only examined regarding size rather than shape. Initially, the NO_x concentration and the air velocity inside the tunnel were set to zero, and no additional vehicles entered the simulation space at $t > 0$. Calculations were run over 30 s in 0.05 s steps. Emissions from the vehicles were set accordingly to the handbook of emission factors of road traffic by the German Environment Agency [35].

The second simulation was run under the same assumptions but included a row of prototype C reactors with an overall active surface 12,000 m^2 at the tube's exit. The 100 reactors were assumed with three 1500 $m^3\,h^{-1}$ ventilators, respectively, and placed on the road's right- and left-hand side (50 reactors on each side). Here, only the airflow was simulated and expressed in several trajectories to assess the amount of turbulence that can be induced across the traffic lanes. In an ideal case, the reactor's air intake should be sufficient to induce circulation over the whole road, homogenizing the concentration profile and ensuring a

high degree of efficiency by lowering transport resistances across the lanes and inside the reactors.

3 Results

3.1 Zero measurement

Data from the zero measurements at 'Rudower Höhe' is listed in Table 1. While workday NO_x pollution levels were consistently higher than average weekend burdens (approximated workday-weekend-ratio for NO: 1.4, for NO_2: 1.2, for NO_x: 1.3), the difference proved to be marginal in CO_2 measurements. However, both value groups showed a sharp concentration increase over the tunnel's length, which confirms the expectations illustrated in Sect. 1. From the lane's entrance to its exit, NO_x levels rose roughly by 580% on workdays and by 650% on the weekend, starting from already elevated levels of 36 ppb (68 µg/m^3) and 23 ppb (43 µg/m^3), respectively. CO_2 concentrations increased by 99% on workdays. Weekend CO_2 data from the exit's container were lost due to instrument failure, but a similar or slightly lower increase was assumed as the middle container showed elevated concentrations comparable to those on workdays. All in all, the air leaving the tunnel proved to be heavily burdened with both NO_x and CO_2 and exhibited a low NO_2/NO-ratio. These findings were in good accordance with the literature [11, 29, 36].

Wind measurement at the tunnel's exit showed a very stable daily air stream profile, where wind speeds seemed to rise and fall with the traffic volume. Thus, velocities also variated between workdays and weekends, as is exemplarily shown in Figure S6 of Online Resource 1 between 19th (Monday) and 25th Jan 2015. Average wind speed on workdays was 4.8 m/s between November and February, ranging from 2 to 8 m/s, whereas air moved with 4 m/s on weekends, ranging from 2 to 5 m/s. Air movement was directed towards the tube exit at all times, with standard derivations (SD) of 5 m/s on workdays and 11 m/s on weekends. Average temperature and humidity were 6.4 °C (SD: 3.8 °C) and 81.7% (SD: 9%).

The NO_x mass flow has been calculated from the average concentration at the tube exit, the wind speed, and the tunnel dimensions of 15 m· 5 m (see Figure S1, Online Resource 1). The mass flow was calculated separately for workdays and weekends, as the former two parameters seemed strongly dependent on this differentiation. The result should be viewed as a rough estimation, given that concentrations were only averaged over one week. As the NO_x consisted of 84% of NO (see Table 1), the NO conversion factor of 1.25 from ppb to µg/m^3 units was used for NO_x as well. Therefore, an estimated NO_x mass flow of 174 mg/s or 15.0 kg/d on workdays and 111 mg/s or 9.6 kg/d on weekends was used for further calculations in this work.

3.2 Lab measurement

The PMMA reactor NO_x measurements are plotted in Fig. 1**.** During the test run, the temperature fluctuated between 20 and 31 °C, while relative humidity ranged from 25 to 40%. The workshop's NO_x levels showed daily variations similar to typical roadside profiles with concentrations around 100 µg/m^3 over the day and around 40 µg/m^3 at night [37].

Under UV-irradiation, a high reduction potential with a deposition velocity of 2 cm/s for NO_x can be attributed to the TiO_2-coated foam material, estimated with 90% degradation. At such a rate, it is to consider that nitrogen dioxide is rapidly depleted inside the sample,

Table 1 Average concentrations from one week of minute-wise data

	Workday average		
	Entrance	Middle	Exit
NO	36	235	328
NO_2	20	41	58
NO_x	56	276	385
CO_2	329	468	654
	Weekend average		
	Entrance	Middle	Exit
NO	23	176	247
NO_2	16	35	49
NO_x	39	211	295
CO_2	332	458	–

Concentrations of every pollutant rose over the tunnel length. All data is given in ppb units

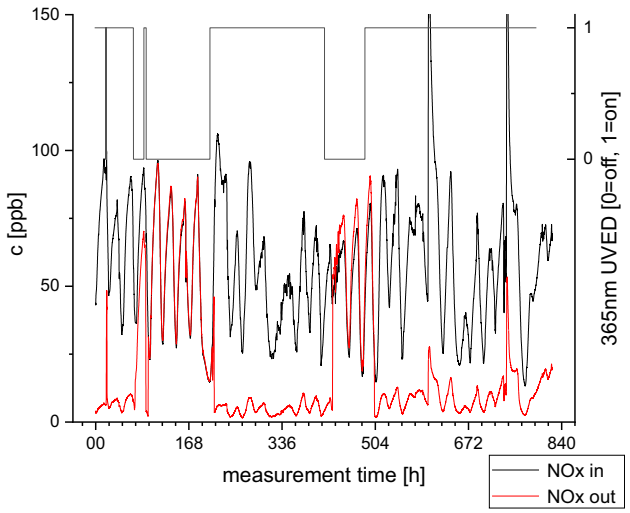

Fig. 1 PMMA reactor measurements for NO_2. A 6.5% decrease in the sensitivity of the input meter was observed over the duration of the long-term test. Since this experiment was not repeatable and the deviation caused an underestimation of the reaction capacities, it was nevertheless taken into consideration

leading to insubstantial amounts and, therefore, more inefficient reduction at the back end of the foam. This could be avoided using a higher flow rate, which would lead to higher NO_x concentrations in the outgoing air but increase the catalyzed NO_x mass per time frame. This follows the same reasoning as the link between NDR and the degree of efficiency, explained in Sect. 2. Since the material had shown no measurable flow resistance (detection limit: 0.5 mbar), greater throughputs seem unproblematic.

IC Analysis was carried out for the time frame between 216 and 432 h and showed a recovery rate of 99%. This underlines the plausibility of the presented method. It also indicated that the reformation of NO_x on the active surfaces does not occur in laboratory conditions, hinting that this problem is somewhat connected to surface passivation or long-term aging [38].

In total, the chosen material seems most suitable for an application, given that strongly polluted air is present at the tunnel's exit and that even a reaction surface of only ~ 0.5 m^2 was able to purify 17 l of air per minute. Yet, known problems such as surface passivation by dust and filth were not addressed in this experiment.

For the long-term experiment, changes in both flexibility of the PU foam and the structural integrity of the TiO_2 coating were monitored. No worsening in performance has been observed throughout the duration of the experiment.

3.3 Reactor geometry influence

The CFD simulations of different material-specific air flows depicted a strong influence of the reaction surface geometry. For a general comparison, all concentrations were normalized to the input concentration.

As mentioned before, the simulation results of prototype A (Fig. 2) could not be readily compared to prototype B. This is further supported by the 10% degree of efficiency shown in Table 2, which illustrates that a volume flow of 30 m^3/h was too low for the reactor's photocatalytic capacities. Nevertheless, various findings caught the eye. On the one hand, RDR was estimated at 97%, so the catalytic processes in prototype A did not seem to be diffusion limited. Yet, the concentration in the inlet stream continued to stay at c_0 until it abruptly fell below 50% c_0 around midway through the reactor, as shown in Fig. 2. This behavior was interpreted as the dissolution of a plug flow that has formed inside the catalytically coated cylindrical mat. As the air in the anterior moves almost entirely inside the cylindrical mat, contact with the photocatalytic surface was unlikely, resulting in low degradation. The degradation was further dampened by a small flow of purified air

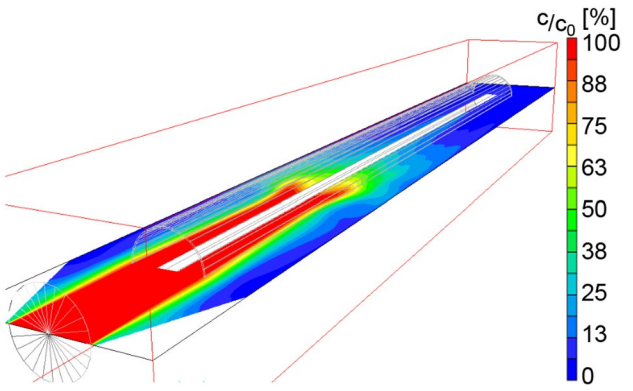

Fig. 2 CFD simulation result for prototype A. Displayed here is a x–z-section of the simulation space shown in Figure S3 of Online Resource 1. All concentrations are given as percentages relative to the uptake concentration

Table 2 Analytically (NDR, degree of efficiency) and numerically (RDR, pressure drop) determined coefficients for all prototypes

	Prototype A	Prototype B
NDR	(99%)	77%
RDR (as proportion of NDR)	(97%)	98%
Degree of efficiency	(10%)	52%
Pressure drop	(-)	33 Pa

Coefficients for prototype B were calculated under different assumptions and cannot be readily compared, as is indicated by brackets

from the outer areas of the prototype to the center, keeping the high concentrations away from the photocatalytic reaction surfaces. Higher simulated and measured volume flows resulted in a longer growing plug flow ending in a flow through the whole prototype, completely dropping the RDR close to zero. Thus, one can assume that this reactor geometry has the optimum of RDR around 30 m^3/h, so that the degree of efficiency was not sufficient for further measurements. Increased volume flow would more likely lead to a sharp decrease of the NDR coefficient, while the expectable RDR decrease would prevent the 'pollution removal mass flow' to rise in the same way. Yet, higher degrees of efficiency may be reached with increased volume flows, provided that the turbulent air stream forms or is induced before the reactor's exhaust.

Simulation results for prototype B are displayed in Fig. 3, which uses another concentration scale than Fig. 2, reaching from 100% c_0 to 70% c_0 instead of 0 c_0. This is not to be interpreted as reduced purification efficiency rather than as a result of flow homogenization due to the foam pads. Such a constant reverse of both flow and concentration differences ensures a high realistic degradation rate (RDR = 98%) by utilizing the whole active surface and reducing transport resistances. Thus, the degree of efficiency of 52% is mainly determined by the decreased c_0 over the active surfaces. An efficiency near 100% may be reached with a sufficiently high-volume flow, as this would result in a pollutant concentration near c_0 in the whole reactor but consequently lower the NDR of 77%.

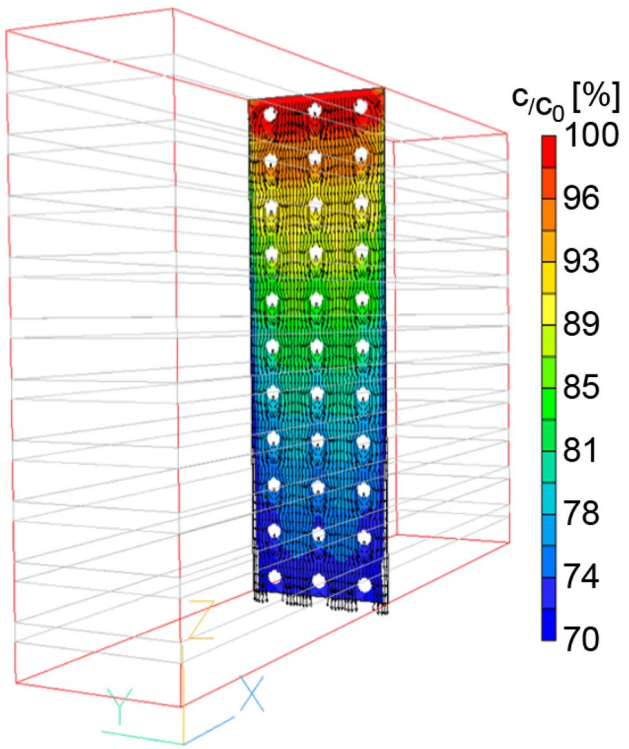

Fig. 3 CFD simulation results for prototype B. Displayed here is a y–z-section of the simulation space shown in Fig. S4 of Online Resource 1. All concentrations are given as percentages relative to the uptake concentration

The porous foam was modeled by a Phoenics software module for perfusable material with the use of a pressure loss coefficient of 8.7 derived from the manufacturers data sheet. Surprisingly, the pressure drop remained low at 33 Pa despite the increased surface-volume ratio, undercutting all 7 simulated reactors, which were initially intended as examples for a passive ventilation approach.

In summary, prototype B showed the most desirable features for an application in the tunnel. As depicted in Table 2, it exhibits a low-pressure drop and the highest RDR. In comparison to prototype A, it reaches a significantly higher surface-to-volume ratio, which could be increased further by filling the whole reactor with TiO_2-carrier material and using UVEDs instead of fluorescence tubes. Moreover, the flow homogenization effect of prototype B would allow increased throughput rates without a sharp decrease in the RDR coefficient, which can be expected for comparable rates in prototype A.

3.4 TUNNEL Concentration and airflow profiles

The Phoenics software displayed simulation results of the tunnel's airflow profile as a *graphics interchange format (GIF),* which can be found in Online Resource 2. The simulation results were discussed based on the profile at t = 29 s with a horizontal section plane and 6 vertical section planes, 50 m apart, respectively (see Figure S7, Online Resource 1). It showed that the induction of turbulence behind a single vehicle is low, as both LDVs in the simulation space's front are pulling a line of fast-moving air behind them, which stay separated from each other. Much more intense turbulence is induced by the following two vehicles behind the second vertical section plane, where air with higher velocities is pushed across multiple lanes by the oncoming traffic. In general, stronger vortex formation and thus lower cross-tube-axis velocity differences can be expected with increasing traffic volume. Wind speeds far from moving vehicles stay below 3 m/s, yet this is perhaps explained by the limited number of LDVs simulated and the short time window, as self-ventilation effects should induce velocities around 5 m/s [39, 40].

Similar behavior could be observed in the simulation of the tunnel's concentration profile animation (see Online Resource 3). In the profile at t = 29 s (see Fig. 4), particularly high pollutant concentrations were found in the right lane, which can be explained by the increased emissions of 1 mg/s NO assumed for HDVs. Those concentration peaks widen towards the tube exit and form wave-like

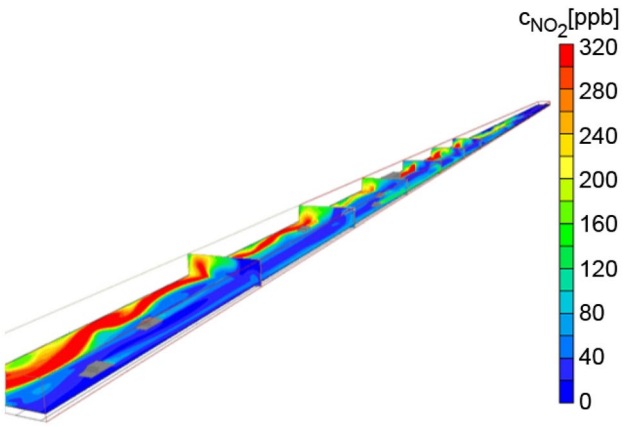

Fig. 4 Concentration profile simulation results at t = 29 s. Wave-like movement of the pollutants flow get more intense towards the tube exit. HDV emissions are considerably higher than LDV emissions

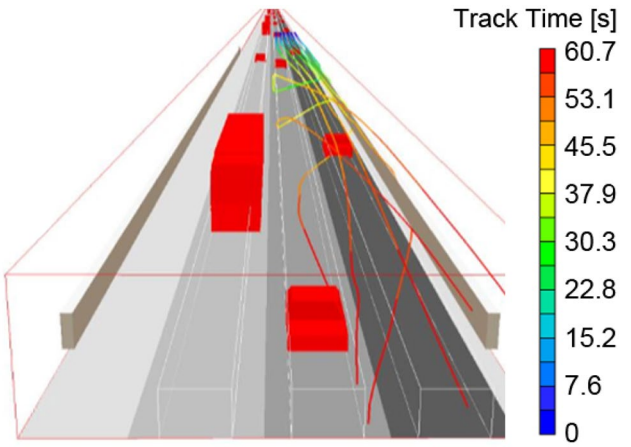

Fig. 5 Air trajectories with reactors at the tube exits. Displayed is the view from the tube's exit (against travel direction). The active ventilation forms a vortex in the airstream of the tunnel. Coloring indicates the trajectories track time

fluctuations yet do not cross over the middle and left-hand lanes. It remained unclear whether higher traffic volumes and more vital vortex formation would level these cross-tube-axis gradients, but for the examined case, the tube's flow properties would not transport polluted air effectively towards reaction surfaces on the tunnel walls.

Figure 5 displays the results of the second CFD simulation, which examined air flow trajectories under the influence of actively vented reactors. For clarity, only the trajectories for the right-hand side of the tube (left-hand side in travel direction) are shown here. Results of the left-hand side were comparable (see Figure S8, Online Resource 1). The trajectories imply a double vortex by active ventilation, where the vortexes have opposite rotation directions. Figure 4 has shown that airflow inside the tube is not turbulent enough to utilize passively vented reaction surfaces. Figure 5 showed that sufficient mass transport is only achieved by active ventilation. It is necessary to place reactors on both sides of the road as complete cross-sectional turbulence is unlikely to be achieved with ventilation on only one side.

In the last step, the on-side reduction potential was roughly assessed. Since active ventilation with 100 reactors (50 on each side set to a volume flow of 450 m^3/h) induce a volume flow of 4,500 m^3/h or 1.25 m^3/s (see Reactor B) seemed capable of transporting air toward the reaction surfaces, the estimation was built upon the ratio between the tunnel's volume flow and the volume flow through the reactors. All calculations were done for workday conditions. 361 m^3 (average airspeed of 4.8 m/s times a tunnel cross-section of 75 m^2) of air left the tunnel every second, while up to 125 m^3/s (100 reactors times 4000 m^3/h or 1.25m^3/s) pass through the reactors. This equals a ratio of 0.346 and can be interpreted as 34.6% of the tunnel air or approximately every third parcel of air flowing over the active surfaces once. This is a vague assumption as different air parcels may pass through multiple reactors, which would cause the degree of efficiency to decrease, as others included in the 34.6% may not flow over TiO_2-surfaces at all. Nevertheless, those processes could not be quantified here and were therefore not considered. The concentration decrease by one reactor passage was calculated using Eq. 18. A single reactor had a photocatalytic active surface of 120 m^2. Furthermore, the average daily concentration of 482 µg/m^3 (386 ppb) was used for c_{in}, again calculated for workdays only. Deposition velocity v_d was assumed from the pure coating, tested according to ISO 22197–2 with 1.4 cm/s.

$$c_{out} = c_{in} \cdot e^{-v_d \cdot \frac{S_{TK}}{V_{TK}}} = 481.9\,\mu g/m^3 \cdot e^{-0.014\,m/s \times \frac{120\,m^2}{1.25\,m^3/s}} = 125.7\,\mu g/m^3 \quad (18)$$

It was further conjectured that the RDR of 98% of the prototype C reactors at 400 m^3/h would not be reduced with the increase of volume flow to 4500 m^3/h, and that its influence could thus be neglected. This conjecture is mainly of mechanical doubts, and as the foam structure is likely to catch dust from the air, it builds up most likely significant pressure drops over time and cumulates in a mechanical destruction of the photocatalytical mats. In an ideal environment, the RDR should rise with higher volume flows, as the catalyst at the outlet of the reactor is supplied with higher concentrations resulting in higher chemical reaction rates. Ultimately, the effect of the pollutant removal efforts was calculated from the mixture of the reactor volume flow of 450,000 m^3/h or

120 m^3/s for all 100 simulated reactors which is a fraction of 34.6% cleaned air with a NO_x burden of 126 µg/m^3 of the overall tunnel flow of 360 m^3/s (75 m^2 tunnel cross section 4.8 m/s average wind speed in the tunnel). An air fraction of 65% leaves the tunnel untreated with concentrations of 482 µg/m^3, resulting in a concentration of around 360 µg/m^3 or a reduction of 25% (122 µg/m^3). Converted into a removal mass flow, considering the tunnel volume flow of 361 m^3/s (tunnel cross-section of 75 m^2 and an average wind speed of 4.8 m/s), this equals a NO_x capture of 44 mg/s or 3.8 kg/day on workdays.

4 Discussion

The results illustrate that on-side reduction of nitrogen oxides at an emission hotspot seems capable to lighten the pollutant burdens of its surroundings. Since the described application in this work aspirated only a third of the air at the tube exit, even higher reduction potentials of 25% seem readily achievable if it is possible to direct all the tunnel's air over an active surface. Moreover, such applications may be implemented in other confined spaces with active NO_x sources.

The utilization of actively vented TiO_2-reactors must be discussed controversially. On one side, their operation would consume energy for both ventilation and UV-irradiation. Depending on the energy mix used, this could lead to the formation of more NO_x than cleaned by the active surfaces. Such a relation resembles observations made in the projection of electric drive-system emission in the future, which will exhibit CO_2, NO_x and SO_2 saving effects only if driven with eco-friendly produced energy [18, 19]. Furthermore, although TiO_2 surfaces catalyse nitrogen oxides and form a sink for them, the energy used for UV irradiation and fans leads to the formation of additional CO_2, depending on the type of electricity production. Yet, the severity of this effect must be accessed quantitatively in further studies, and could perhaps be neglected, if ventilation is operated with alternative energy, such as solar power. Independently of these considerations, such measures may become necessary to protect human health. In this regard, the method outlined is an end-of-pipe technology since it captures pollutants in a confined space directly before their release into the open atmosphere.

On the other hand, active ventilation bears several advantages. By lowering the transport resistances, high efficiency can be expected, as shown for prototype B in Table 2. Additionally, the formation of nitric acid [26] takes place in a confined space, and thus can be periodically washed from the active surfaces and transferred to wastewater treatment facilities. In this way, specific soil acidification and eutrophication potential can be retained because atmospheric NO_x forms HNO_3 as well [8]. Washing may also contribute to the durability of the TiO_2-coated materials since surface passivation is a significant problem in highly polluted spaces [21, 28], and sufficient wash-off by rain cannot be expected in a tunnel. Finally, the separation of the active surfaces from the open tunnel space allows the use of various carrier materials, such as foam structures. Those carriers do not only have high surface-to-volume-ratios, which benefits were illustrated by the CFD simulation of prototype C and Eq. 16, that shows the direct link between surface area and pollutant reduction. The materials in use can also be designed to retain a high degree of activity under periodic washing, whereas the catalytic activity of TiO_2 on concrete carrier materials decreases after repeated wetting [24]. If surface reactivation by washing proves inefficient, the foam structures could as well be easily exchanged periodically.

Some decisive factors for implementation have been identified. For once, minimization of diffusion barriers inside the reactor and the induction of out-side convection toward the reactors is essential for a sufficient pollutant flow onto the active surfaces. Steep concentration gradients and large mass transports can be achieved by high flow velocities and thus strong ventilation. As the latter is mostly defining the methods of energy demand, it becomes a criterion of optimization. Upon a given NO_x burden, it may be more suitable to shut down several reactors but increase the volume flow through the others, or vice versa, to operate the ventilators in their optimal performance range. Ultimately, the placement of the reactors in the tunnel or the hotspot in question is determined for the resulting air stream, which determines the removal mass. Therefore, it is recommended to simulate the arising flow beforehand and optimize the location of the reactors.

Several issues have not been examined in this work. Future studies should investigate the influence of the carrier materials' geometry, durability, and surface reactivation capabilities more closely. A porosity of 5 ppi showed beneficial properties in both laboratory and simulation test, yet more pores per inch will lead to a drastically increased surface area but heighten the pressure drop and thus the energy consumption and hinder an efficient irradiation. Furthermore, durable carriers and reactivatable surfaces may lower costs and the ecological footprint of the method itself. The durability of PU foam was tested for 6 weeks here, whereas it remains in question if surface activation is possible. Two more points need to be addressed before the technology outlined can be used. It is crucial to assess the emissions connected to its operation, especially regarding carrier production, TiO_2 coating, energy demand, and surface reactivation efforts. In this way, the expense of the method can be compared to its benefit. To identify

problems under real-world conditions and shortcomings of the observations presented here, a field test of the method is equally important.

5 Conclusion

We investigated the applicability of photocatalytic reactors for air purification in large road tunnels with heavy traffic. Our measurements and simulations show that the method can neutralize significant amounts of pollutants. For efficient operation, it is necessary to design the reactors internally in such a way that a maximum reaction surface is achieved and at the same time a high flowability is given. Furthermore, the reactors must be mounted to match the tunnel geometry so that (a) a maximum concentration of pollutant gas hits the catalyst surfaces and (b) the complete tunnel air can reach the reactors before exiting the tunnel. The possibility of reducing the amount of pollutant gases that a tunnel emits into the atmosphere can be considered in the approval of new tunnel facilities to prevent limit values from being exceeded.

The photocatalytic coating used in this study was brittle and thus challenging in its handling. Ongoing research should focus on material development to combine a strong photocatalytic effect with usual coating properties. Automated cleaning of the photocatalysts could not be considered in this study, but for the long-term operation of the reactors, a washing device should be integrated. A future study investigating the influence of the internal foam structure could lead to an optimized balance between reaction surface, pressure drop and reaction surface irradiation, to minimize the amount of energy required to operate the ventilation and irradiation in such reactors. The increasingly widespread use of very compact semiconductor emitters in the UV range can be exploited in future studies to significantly increase the reaction surface area per reactor volume, resulting in a significant increase in their efficiency.

Acknowledgements Special thank goes to the tunnel management of the Berlin Senate, which has always helped in a committed and uncomplicated way and contributed to making the measurements in the tunnel possible.

Author contributions CE and DS designed and performed the study; CE and MF surveyed the literature; CE and MF wrote the first draft of the manuscript; CE and TF designed CFD simulations; TF performed CFD simulations; TF and DS contributed to data interpretation and revised the manuscript.

Funding Open Access funding enabled and organized by Projekt DEAL. This study was funded by the German Federal Highway Research Institute (BASt) (Grant Number FE 09.0184/2011/ARB).

Declarations

Conflict of interest Clemens Ehm declares that he has no conflict of interest. Max Frohmüller declares that he has no conflict of interests. Dietmar Stephan declares that he has no conflict of interest. Thomas Flassak declares that he has no conflict of interest.

Ethical approval This article does not contain any studies with human participants or animals performed by any of the authors.

References

1. Malley CS et al (2018) Analysis of the distributions of hourly NO_2 concentrations contributing to annual average no_2 concentrations across The European Monitoring Network between 2000 And 2014. Atmos Chem Phys 18:3563–3587. https://doi.org/10.5194/Acp-18-3563-2018
2. Minkos A, Dauert U, Feigenspan S Et Al. (2020) Air quality 2019. German Environment Agency, Dessau-Roßlau, Germany
3. EEA (2019) Air Quality in Europe: 2019 Report. EEA Report No. 10/2019. Publications Office Of The European Union, Luxembourg
4. Institut Für Arbeitsschutz Der Deutschen Gesetzlichen Unfallversicherung (2019) Gestis Datenbank: Ozon. http://gestis.itrust.de
5. Institut Für Arbeitsschutz Der Deutschen Gesetzlichen Unfallversicherung (2019) Gestis Datenbank: Stickstoffmonoxid. http://gestis.itrust.de
6. WHO (2013) Review of evidence on health aspects of air pollution—Revihaap 12. 2020. Project: Final Technical Report. Copenhagen, Denmark
7. U.S. EPA (2016) Integrated science assessment for oxides of nitrogen–health criteria. U.S. EPA, Washington DC
8. Atkinson R (2000) Atmospheric chemistry of VOCs and No_x. Atmos Environ 34:2063–2101. https://doi.org/10.1016/S1352-2310(99)00460-4
9. Jacobson MZ (2012) Air pollution and global warming: history, science, and solutions, 2nd edn. Cambridge University Press, Cambridge
10. Nuvolone D, Petri D, Voller F (2018) The effects of ozone on human health. Environ Sci Pollut Res Int 25:8074–8088. https://doi.org/10.1007/S11356-017-9239-3
11. National Center for Environmental Assessment, NCEA-RTP (2013) Integrated science assessment for ozone and related photochemical oxidants: EPA/600/R-10/076F, Washington DC

12. EEA (2014) Air quality in Europe. EEA Report, vol 2014, 5. European Environment Agency, Copenhagen
13. Cheval S, Mihai Adamescu C, Georgiadis T et al (2020) Observed and potential impacts of the covid-19 pandemic on the environment. Int J Environ Res Public Health. https://doi.org/10.3390/Ijerph17114140
14. Gautam S (2020) Covid-19: air pollution remains low as people stay at home. Air Qual Atmos Health. https://doi.org/10.1007/S11869-020-00842-6
15. Higham JE, Ramírez CA, Green MA et al (2020) UK Covid-19 lockdown: 100 days of air pollution reduction? Air Qual Atmos Health. https://doi.org/10.1007/S11869-020-00937-0
16. Muhammad S, Long X, Salman M (2020) Covid-19 pandemic and environmental pollution: a blessing in disguise? Sci Total Environ 728:138820. https://doi.org/10.1016/J.Scitotenv.2020.138820
17. Yan F, Winijkul E, Streets DG et al (2014) Global emission projections for the transportation sector using dynamic technology modeling. Atmos Chem Phys 14:5709–5733. https://doi.org/10.5194/Acp-14-5709-2014
18. Keshavarzmohammadian A, Dk H, Jb M (2017) Emission impacts of electric vehicles in the US Transportation Sector following optimistic cost and efficiency projections. Environ Sci Technol 51:6665–6673. https://doi.org/10.1021/Acs.Est.6b04801
19. Rietmann N, Hügler B, Lieven T (2020) Forecasting the trajectory of electric vehicle sales and the consequences for worldwide CO_2 emissions. J Clean Prod 261:121038. https://doi.org/10.1016/J.Jclepro.2020.121038
20. Serpone N, Av E (2012) Semiconductor photocatalysis—past, present, and future outlook. J Phys Chem Lett 3:673–677. https://doi.org/10.1021/Jz300071j
21. Serpone N (2018) Heterogeneous photocatalysis and prospects of TiO_2-based photocatalytic denoxing the atmospheric environment. Catalysts 8:553. https://doi.org/10.3390/Catal8110553
22. Chen J, Kou S, Poon C (2011) Photocatalytic cement-based materials: comparison of nitrogen oxides and toluene removal potentials and evaluation of self-cleaning performance. Building Environ 46:1827–1833. https://doi.org/10.1016/J.Buildenv.2011.03.004
23. Martin M, Leonid S, Tomáš R et al (2017) Anatase TiO_2 nanotube arrays and titania films on titanium mesh for photocatalytic No_x removal and water cleaning. Catal Today 287:59–64. https://doi.org/10.1016/J.Cattod.2016.10.011
24. Seo D, Yun TS (2017) Nox removal rate of photocatalytic cementitious materials with TiO_2 in wet condition. Building Environ 112:233–240. https://doi.org/10.1016/J.Buildenv.2016.11.037
25. Folli A, Pade C, Hansen TB et al (2012) TiO_2 photocatalysis in cementitious systems: insights into self-cleaning and depollution chemistry. Cem Concr Res 42:539–548. https://doi.org/10.1016/J.Cemconres.2011.12.001
26. Laufs S, Burgeth G, Duttlinger W et al (2010) Conversion of nitrogen oxides on commercial photocatalytic dispersion paints. Atmos Environ 44:2341–2349. https://doi.org/10.1016/J.Atmosenv.2010.03.038
27. Pérez-Nicolás M, Navarro-Blasco I, Fernández JM et al (2017) Atmospheric No_x removal: study of cement mortars with iron- and vanadium-doped TiO_2 as visible light–sensitive photocatalysts. Constr Build Mater 149:257–271. https://doi.org/10.1016/J.Conbuildmat.2017.05.132
28. Gallus M, Akylas V, Barmpas F et al (2015) Photocatalytic depollution in the Leopold II tunnel in brussels: Nox abatement results. Build Environ 84:125–133. https://doi.org/10.1016/J.Buildenv.2014.10.032
29. Simmons WA, Pw S (2012) Estimations of primary nitrogen dioxide exhaust emissions from chemiluminescence NO_x measurements in a UK road tunnel. Sci Total Environ 438:248–259. https://doi.org/10.1016/J.Scitotenv.2012.08.050
30. Longley I, Kelly F (2008) Air quality in and around traffic tunnels: final report. National Health and Medical Research Council, Canberra
31. Forschungsgesellschaft Für Straßen- Und Verkehrswesen (2010) Richtlinien Für Die Ausstattung Und Den Betrieb Von Straßentunneln: Rabt, Ausg. 2006, Korrigierter Nachdr. Fgsv, vol 339. Fgsv-Verl., Köln
32. Bast (2015) Federal road information system. https://www.bast.de/bast_2017/de/verkehrstechnik/fachthemen/v2-verkehrszaehlung/verkehrszaehlung.html?nn=1817946. Accessed 17 Dec 2020
33. Cham (2015) Phoenics CFD. Concentration. Heat & Momentum Limited, London
34. Minero C, Bedini A, Minella M (2013) On the standardization of the photocatalytic gas/solid tests. Int J Chem Reactor Eng 11:717–732. https://doi.org/10.1515/Ijcre-2012-0045
35. Knörr W, Hausberger S, Steven H (2004) Handbuch Der Emissionsfaktoren Des Strassenverkehrs 2.1. INFRAS, Bern
36. Kristensson A, Johansson C, Westerholm R et al (2004) Real-world traffic emission factors of gases and particles measured in a road tunnel in Stockholm, Sweden. Atmos Environ 38:657–673. https://doi.org/10.1016/J.Atmosenv.2003.10.030
37. Pandey SK, Kim K-H, Chung S-Y et al (2008) Long-term study of NO_x behavior at urban roadside and background locations in Seoul, Korea. Atmos Environ 42:607–622. https://doi.org/10.1016/J.Atmosenv.2007.10.015
38. Bloh JZ, Marschall R (2017) Heterogeneous photoredox catalysis: reactions, materials, and reaction engineering. Eur J Org Chem:2085–2094. https://doi.org/10.1002/Ejoc.201601591
39. Herzke K (1972) Der Einfluß Des Kraftfahrzeugverkehrs Auf Die Betriebskosten Von Tunnellüftungen. von Kurt Herzke Berlin, Berlin
40. ASTRA (2008) LÜFTUNG Der Straßentunnel: Systemwahl, Dimensionierung Und Ausstattung, V2.01. ASTRA, Bern